



Published in final edited form as:

Nat Genet. 2013 March ; 45(3): 285–289. doi:10.1038/ng.2526.

Genomic sequencing of meningiomas identifies oncogenic *SMO* and *AKT1* mutations

Priscilla K. Brastianos^{a,1,2,3,4}, Peleg M. Horowitz^{a,3,4,5,6}, Sandro Santagata^{3,7}, Robert T. Jones^{1,8}, Aaron McKenna⁴, Gad Getz⁴, Keith L. Ligon^{3,7}, Emanuele Palescandolo⁸, Paul Van Hummelen^{1,8}, Matthew D. Ducar^{1,8}, Alina Raza^{1,8}, Ashwini Sunkavalli^{1,8}, Laura E. MacConaill^{1,8}, Anat O. Stemmer-Rachamimov^{3,9}, David N. Louis^{3,9}, William C. Hahn^{b,1,3,4,8}, Ian F. Dunn^{b,3,6}, and Rameen Beroukhim^{b,1,3,4,5,8}

¹Department of Medical Oncology, Dana-Farber Cancer Institute

²Department of Medical Oncology, Massachusetts General Hospital

³Harvard Medical School

⁴Broad Institute of MIT and Harvard

⁵Department of Cancer Biology, Dana-Farber Cancer Institute

⁶Department of Neurosurgery, Brigham and Women's Hospital

⁷Department of Pathology, Brigham and Women's Hospital

⁸Center for Cancer Genome Discovery, Dana-Farber Cancer Institute

⁹Pathology Service and Cancer Center, Massachusetts General Hospital

Abstract

Meningiomas are the most common primary nervous system tumor. The tumor suppressor *NF2* is disrupted in approximately half of meningiomas¹ but the complete spectrum of genetic changes remains undefined. We performed whole-genome or whole-exome sequencing on 17 meningiomas and focused sequencing on an additional 48 tumors to identify and validate somatic genetic alterations. Most meningiomas exhibited simple genomes, with fewer mutations, rearrangements,

Users may view, print, copy, download and text and data- mine the content in such documents, for the purposes of academic research, subject always to the full Conditions of use: http://www.nature.com/authors/editorial_policies/license.html#terms

^b**Correspondence**, Rameen Beroukhim (rameen@broadinstitute.org), Ian Dunn (idunn@partners.org), William Hahn (william_hahn@dfci.harvard.edu), Dana-Farber Cancer Institute, 450 Brookline Avenue, Boston, MA 02215.

^aCo-first authors

ACCESSION CODES

Data, including sequence data and analyses, are available for download via dbGaP (http://www.ncbi.nlm.nih.gov/projects/gap/cgi-bin/study.cgi?study_id=phs000552.v1.p1).

AUTHOR CONTRIBUTIONS

P.K.B., P.M.H., I.F.D., R.B. and W.C.H. conceived the study, designed the experiments, analyzed the data and wrote the paper. P.M.H. performed the bio-informatic analyses, and A.M., G.G., R.B. and M.D.D. provided analytical advice. S.S., A.O.S.R., and D.N.L. reviewed the histopathology and S.S. performed immunohistochemistry. K.L.L. managed the tissue repository. R.T.J., E.P., P.V.H., A.R., A.S. and L.E.M. provided technical support and performed sequencing. W.C.H., I.F.D., and R.B. supervised the study. All authors discussed the results and implications and commented on the manuscript.

COMPETING FINANCIAL INTERESTS

WCH is a consultant for Blueprint Medicines and Thermo Fisher. RB is a shareholder for AstraZeneca. WCH and RB are consultants for and receive research support from Novartis.

and copy-number alterations than reported in other adult tumors. However, several meningiomas harbored more complex patterns of copy-number changes and rearrangements including one tumor with chromothripsis. We confirmed focal *NF2* inactivation in 43% of tumors and found alterations in epigenetic modifiers among an additional 8% of tumors. A subset of meningiomas lacking *NF2* alterations harbored recurrent oncogenic mutations in *AKT1* (E17K) and *SMO* (W535L) and exhibited immunohistochemical evidence of activation of their pathways. These mutations were present in therapeutically challenging tumors of the skull base and higher grade. These results begin to define the spectrum of genetic alterations in meningiomas and identify potential therapeutic targets.

Meningiomas, tumors that arise from arachnoidal cap cells of the leptomeninges, constitute approximately one-third of primary central nervous system (CNS) tumors¹. Most meningiomas (80%) are World Health Organization (WHO) grade I and treated by surgical resection. However, resection of some meningiomas, particularly at the skull base, is associated with high morbidity. Moreover, 18% of these will recur within five years, and patients with grade I tumors have significantly reduced long-term survival related to both tumor recurrence and stroke risk². Recurrence rates for grade II and III meningiomas can be as high as 40% and 80%, with 5-year overall survival of approximately 76% and 32%, respectively^{1,3,4}. Although there are recent reports of a stepwise progression of a subset of grade I meningiomas to higher grades^{5,6}, these secondary grade II/III meningiomas may differ fundamentally from spontaneously arising grade II/III tumors. Radiation is frequently used as an adjunct to surgery; however, there are no effective chemotherapeutic options when surgery and radiation fail to offer durable long-term disease control⁷.

We sequenced DNA from a discovery set of grade I meningiomas using whole-genome (n = 11) and whole-exome (n = 6) techniques to identify somatic copy-number alterations (SCNAs), rearrangements, mutations, and insertions/deletions throughout the genome. We then sequenced 645 known cancer-associated genes, including genes altered in this discovery set, in a validation set of 30 additional grade I tumors. We also sequenced these genes in an extrapolation set of 18 grade II-III meningiomas to evaluate whether findings in grade I tumors extended to the tumors of higher grades (Online Methods, Supplementary Tables 1 and 2).

Meningiomas in the discovery set exhibited a small number of somatic genetic events compared to other tumor types⁸⁻¹⁴. We sequenced to high depth (median 57X genome, 181X exome, and 154X validation/extrapolation coverage) and utilized large-insert libraries in whole-genome samples (500 bp and 800 bp) to optimize our detection of rearrangements and other events. Nevertheless, we found that the median meningioma exhibited SCNAs affecting only 3.3% of the genome, one rearrangement, and 8 non-synonymous mutations. Among mutations, cytosine to thymidine transitions within a CpG context predominated, consistent with spontaneous deamination (Supplementary Fig. 1a)¹⁵. The rates of alteration we observed in meningiomas were significantly lower (often by a factor of 10 or more) than previously determined rates for other tumors that have been sequenced to lower depth and with smaller insert sizes (Fig. 1a-c). These findings may reflect differences in mitotic index, prior treatments, or carcinogen exposure between these tumor types.

In contrast, rates of genomic disruption were higher among the grade II-III meningiomas in the extrapolation set than their grade I counterparts (Supplementary Fig. 2). The mean rate of non-synonymous mutations within the 645 sequenced genes was nearly twice as high in higher-grade tumors (3.0 vs. 1.6; $p < 0.02$), and the proportion of the genome affected by SCNAs was dramatically higher (median 12.8 vs. 0.3%; $p < 0.001$).

Among SCNAs, loss of chromosome 22 (containing *NF2*) was the most frequent genetic alteration in the discovery cohort, occurring in all 10 tumors with focal *NF2* alteration (defined as mutation, insertion/deletion, or rearrangement within the *NF2* locus) and one without (Fig. 1d, Supplementary Fig. 3). The association between *NF2* mutation and chr22 loss extended to the validation and extrapolation sets ($p < 0.0001$) and confirms prior reports using other methods¹⁶. In the grade I tumors, we also found recurrent significant losses on 1p, 7p, 14p, and 19 and gains on chr5 and chr20 ($q < 0.1$), some of which have been described previously¹⁷. Higher-grade tumors of the extrapolation set exhibited additional recurrent losses on 10q and 14q, previously reported in atypical and anaplastic meningiomas¹. We did not observe previously described losses of *DAL-1*, a gene related to *NF2* on 18p¹⁸.

We identified a total of 110 candidate somatic rearrangements in whole-genome samples, of which 93 were confirmed to have reads spanning the putative fusion site (Supplementary Table 3, Supplementary Fig. 4). Most of these were concentrated in three tumors (Fig. 2), one of which exhibited chromothripsis, a simultaneous rearrangement of one or more chromosomes estimated to occur in 2–3% of aggressive malignancies^{19,20}. One of the genes disrupted by chromothripsis was the putative tumor suppressor *NEGR1*, which was also rearranged in a second tumor. *NEGR1* plays a role in CNS development and is recurrently deleted in neuroblastoma²¹, though its role in tumorigenesis remains to be elucidated. A third sample harbored disruptions in the known and putative tumor suppressors *NF1*, *NF2*, and *CDK14*. A copy-neutral 12.5Mb inversion caused reciprocal fusion of *NF2* (before exon 2) and *TCF20*, representing a novel mechanism of inactivating *NF2* in meningiomas. We also identified other translocations in samples that were not subjected to whole-genome analysis, including a truncating translocation in *CHEK2* (Supplementary Fig. 4i and Supplementary Table 3). The loss of *CHEK2* may lead to impaired DNA repair, as has been described in meningioma cell lines²².

The most frequently mutated gene was *NF2*, which exhibited a total of nine nonsense mutations, nine splice site mutations, nine frame-shift insertions-deletions, and the above-mentioned translocation (Supplementary Fig. 5). The majority of these events overlap with previously reported events, and our rates of *NF2* inactivation are consistent with published rates¹. The non-synonymous mutation rates of tumors with and without focal *NF2* alterations did not differ significantly, nor did the spectra of their mutation subtypes (Supplementary Fig. 1b–d).

We also identified non-synonymous mutations in 190 other genes (Supplementary Tables 4 and 5). We determined the significance of mutation rates in individual genes relative to genome-wide background rates. Six genes reached statistical significance (Fig. 3, Supplementary Fig. 5, Supplementary Table 4). Four of these (*NF2*, *KDM5C*, *SMO*, and

AKT1) have previously been implicated in cancer, and the other two (*RGPD3* and *CD300C*) have not. Isolated or rare mutations that did not reach significance across the entire cohort were observed in 23 genes with known involvement in cancer, including *TP53*, *APC*, *CBL*, *STK11* and *NOTCH2*.

Among genes mutated in our cohort and previously associated with cancer, three (*KDM5C*, *KDM6A*, and *SMARCB1*) are epigenetic modifiers. Mutations involving these genes affected 8% of the cohort. Both *KDM5C* (also known as *JARID1C*) and *KDM6A* are histone demethylases²³; *SMARCB1* (also named *SNF5* and *INI1*) is a member of the SWI/SNF chromatin-remodeling complex. *SMARCB1* is located 6 Mb from *NF2*, and a “four hit” model of biallelic inactivation of both genes has been described in familial schwannomas²⁴. The mutation we identified (R374Q) is near a mutational hotspot (R377H) described in meningiomas²⁵ and germline mutations in *SMARCB1*, including R374Q, have been reported in the congenital disorder, Coffin-Siris syndrome²⁶.

We observed mutations of *SMO*, a member of the Hedgehog (Hh) signaling pathway, in three tumors (5%). None of these tumors exhibited focal alterations of *NF2*. Two samples harbored *SMO* W535L, a known oncogenic mutation in basal cell carcinomas²⁷, and a third harbored an L412F mutation, previously reported in desmoplastic medulloblastoma²⁸. The allelic fractions of these mutations (45%, 55% and 47%) were among the highest in these tumors, suggesting clonality. Moreover, dysregulation of the Hh pathway has been previously described in meningiomas^{29,30}. Gorlin syndrome (nevroid basal-cell carcinoma syndrome) is caused by a germline *PTCH1* mutation (upstream of *SMO*), and is characterized by predisposition to multiple cancers, including desmoplastic medulloblastomas and meningiomas^{31,32}. Although we did not observe somatic mutations in *PTCH1*, two samples harbored germline alterations that were also present in the tumor (D436N, E44G/P1282L). However, these patients did not exhibit manifestations of Gorlin syndrome, so the functional significance of these specific events is unclear.

Six samples exhibited mutations of the PI3K/AKT/mTOR pathway. None of these had mutations of *NF2* or *SMO* ($p=0.03$). Five samples harbored identical *AKT1* mutations (E17K) known to be oncogenic in breast, colorectal and lung cancers³³. The E to K substitution results in constitutive AKT1 activation, which stimulates downstream mTOR signaling. The sixth sample exhibited a novel *MTOR* mutation (D1279V).

The Hh and PI3K pathway mutations were also associated with particular histopathologic subtypes (Fig. 4). *SMO*- and *AKT1/MTOR*- mutated meningiomas were predominantly of the meningothelial subtype ($p=0.009$, $p=0.005$, Fisher’s exact test). This is in contrast to the grade I *NF2*-altered tumors, which were predominantly fibroblastic and/or transitional ($p=0.013$), consistent with prior reports³⁴. We did not find statistically significant correlations with other clinically relevant variables including age, location or prior resection. However, one *AKT1*- and two *SMO*-mutated tumors were resected from the skull base, a region that offers particular challenges to resection and higher rate of recurrence³⁵ (Supplementary Table 5).

To validate these findings, we also genotyped an additional 46 grade I and 49 grade II/III meningiomas for *AKT1* (E17K) and *SMO* (W535L and L412F) mutations using a mass spectrometric based method (Sequenom hME). We found one *SMO* (L412F) mutation and three additional *AKT1* (E17K) mutations (Supplementary Table 6). One of these was in a grade III tumor, and the remaining three were in skull base tumors, of which two were of meningothelial histology.

Mutations in *SMO*, *AKT1*, and *MTOR* also correlated with markers of pathway activation. GAB1 immunoreactivity is used in medulloblastomas to characterize tumors with Hh pathway activation³⁶. Among the 65 meningiomas, seven exhibited strong immunoreactivity for GAB1, including the three tumors harboring *SMO* mutations ($p=0.0008$). The other four GAB1-positive tumors were grade II meningiomas. Likewise, STMN1 expression is a marker of PI3K/Akt pathway activation³⁷. Ten meningiomas exhibited strong STMN1 expression, including all six *AKT1* and *MTOR*-mutated meningiomas ($p=3\times 10^{-6}$). Notably, all three *SMO*-mutated meningiomas also exhibited strong ($n=2$) or moderate (1) STMN1 staining. This is consistent with studies that have suggested that Hh and PI3K/AKT/mTOR pathways may interact³⁸.

We observed recurrent mutations in signaling pathways and epigenetic modifiers, but our data also highlight the heterogeneity of mutations in these tumors. Among the 17 tumors we comprehensively characterized, three (18%) did not exhibit mutations in any of the significantly mutated genes. Genomic characterization of additional tumors, particularly of higher grades, is likely to reveal additional oncogenic mechanisms.

These observations also have the potential to guide new therapeutic strategies. We observed *SMO* and *AKT1* mutations in tumors that pose special therapeutic challenges, including a high-grade and six skull-base tumors. Inhibitors of SMO have generated high response rates in patients with basal cell carcinoma, many of which are driven by Hh pathway mutations³⁹. Likewise, inhibitors of the PI3K/AKT/mTOR pathway have shown promise in preclinical and clinical trials in multiple cancer types⁴⁰. The paucity of additional genetic events in meningiomas harboring mutations of PI3K and Hh signaling pathways suggests that patients with these meningiomas may benefit from such targeted therapies already in development or use.

ONLINE METHODS

Sample Selection and Preparation

This study was reviewed and approved by the human subjects institutional review boards of the Dana-Farber Cancer Institute, Brigham and Women's Hospital, and the Broad Institute of Harvard and MIT. Written informed consent was obtained from all participants. We chose to initially perform whole-exome sequencing in 6 meningiomas as a pilot study to determine the optimal depth of whole-genome sequencing needed to provide adequate tumor coverage in spite of stromal contamination. These six tumors and 11 additional whole-genome sequenced meningiomas comprised the discovery cohort. To validate clinically actionable mutations identified in the discovery set, we performed focused sequencing on a validation cohort consisting of an additional 30 grade I meningiomas. We also assembled an

extrapolation cohort of 15 grade II and 3 grade III meningiomas (Supplementary Table 1) in order to compare genetic aberrations of low- and high-grade tumors. Our approach of deep, broad sequencing of a small representative cohort followed by validation in an independent larger group is similar to the approach used by others to discover *IDH1*⁴¹ and *PIK3CA*⁴² mutations. Three study pathologists (SS/DL/ASR) reviewed the histopathologic diagnosis, grade and purity of each tumor.

Representative fresh-frozen blocks with estimated purity of ~90% were selected. DNA was extracted from tissue shavings and buffy coat preparations of paired blood using standard techniques (QIAGEN, Valencia CA) then quantified using PicoGreen® dye (Invitrogen, Carlsbad CA). Identities of tumor-normal pairs were confirmed by mass spectrometric genotyping using a well-established 48-SNP panel (Sequenom, San Diego CA)⁴³.

Data, including sequence data and analyses, are available for download via dbGaP (http://www.ncbi.nlm.nih.gov/projects/gap/cgi-bin/study.cgi?study_id=phs000552.v1.p1).

Sequencing

For whole-genome sequencing (n=11), DNA was randomly fragmented and libraries of two insert sizes were prepared (500 and 800bp) for paired-end sequencing on Illumina HiSeq 2000^{10,11}. Target depth (60X-tumor/30X-normal) was achieved in all but one sample (MEN0015) that failed 800bp library preparation; however, adequate coverage of the 500bp library was achieved.

For whole-exome sequencing (n=6), 250bp libraries were prepared by Covaris sonication (Covaris, Woburn MA), followed by double size-selection (Agencourt AMPure XP beads) and ligation to specific barcoded adaptors (Illumina TruSeq) for multiplexed analysis. Exome hybrid capture was performed with NimbleGen SeqCap EZ Exome Library SR v2.2, Agilent Sure Select All Exon v2.0 hybrid capture kit, or both approaches. All samples but one achieved >150X coverage in exon regions (MENex004, 79X-tumor/90X-normal).

We proceeded with sequencing 645 cancer-associated genes in our larger validation and extrapolation sample set (n=48) because this pre-selected gene set (OncoPanel) included all genes of interest that were also clinically actionable (including *AKT* and *SMO*) that arose in the discovery set. In addition, a wide breadth of other genes in the same families (such as *MTOR* in the *AKT* pathway) and other interesting cancer-related genes in other families were included (Supplementary Table 2). Briefly, DNA was sonicated to achieve an average fragment size of 150bp, then size-selected and barcoded as above. Each multiplexed pool was hybridized with biotinylated baits (Agilent SureSelect, Agilent) designed to capture exonic sequences. Streptavidin-coated beads were used to pull down the complexes, which were loaded on a HiSeq2000 for paired-end sequencing.

Sequencing Analysis Pipeline

For exome- and OncoPanel-sequenced data, pooled sample reads were de-multiplexed using Picard tools (<http://picard.sourceforge.net>). Read pairs were aligned to the hg19 reference sequence (b37) (<ftp://ftp-trace.ncbi.nih.gov/1000genomes/ftp/technical/reference/>) using the Burrows-Wheeler Aligner⁴⁴ (<http://bio-bwa.sourceforge.net/bwa.shtml>) with options: -q 5 -l

32 -k 2 -o 1. Data were sorted and duplicate-marked using Samtools (<http://samtools.sourceforge.net>) and Picard. Bias in base quality score assignments due to flowcell, lane, dinucleotide context, and machine cycle were analyzed and recalibrated, and local realignment around insertions/deletions was achieved using the Genome Analysis Toolkit (GATK) (<http://www.broadinstitute.org/gatk/>)^{45,46}.

Variant and germline calling were performed within the Firehose environment¹¹ using GenePattern⁴⁷. All algorithms described are available publicly (<https://confluence.broadinstitute.org/display/CGATools>). All sample pairs passed a QC pipeline to test for any tumor/normal and inter-individual mix-ups by comparing insert-size distribution and copy-number profile as described previously¹⁰. The Mann-Whitney test was used to determine significance of differences between rates of somatic genetic alteration between meningiomas and the other datasets.

Somatic copy-number alterations (SCNAs) and rearrangements

SCNAs were evaluated using SegSeq⁴⁸, which uses a combination of local change-point analysis and subsequent merging of adjacent chromosomal segments with similar copy-number. For arm-level significance analysis, pseudo-markers were added every 10,000 bases to segmented copy-number data, and these were analyzed by GISTIC 2.0 to determine which events occurred more often than expected by chance¹⁴.

Rearrangements and their exact breakpoints were identified using the combination of dRanger and BreakPointer algorithms^{8,10}. Briefly, dRanger identifies potential rearrangements from read pairs mapping to different chromosomes or unexpected positions / orientations on the same chromosome, and BreakPointer locates reads spanning the fusion and maps the exact breakpoint using modified Smith-Waterman alignment¹⁰.

Rearrangements are assigned a score reflecting the number of tumor reads supporting a breakpoint, the fraction of nearby reads with MAPQ0, the prevalence of other nearby discordant pairs, and the standard deviation of breakpoint starting positions. To minimize false-positive rearrangements, only breakpoints with score ≥ 8 passing BreakPointer were accepted. The specificity of this type of approach has previously been shown to be $>90\%$ ¹⁰. Copy-number and rearrangement results were displayed using the Circos program (<http://mkweb.bcgsc.ca/circos>)⁴⁹.

Identification of base pair substitutions and short insertion-deletions

Mutations were only considered at covered positions ($\geq 8X$ -normal and $14X$ -tumor sites). Somatic mutations and short insertions/deletions were called and post-filtered using MuTect and IndelLocator^{10,11}. These were annotated to genes and compared to events in the Catalogue of Somatic Mutations in Cancer (COSMIC) using Oncotator, and spurious calls caused by mis-mapping and other previously identified systematic errors were removed using an established list of known problematic sites¹¹⁻¹³. MutSig was used to determine the significance of mutated genes, adjusting for cohort- and genome-wide mutation rate, local background mutation rate, and gene length¹¹⁻¹³. We used a cohort-wide background mutation rate instead of the more commonly used sample-specific mutation rate because the observed low mutation rate in these tumors leads to poor sampling of individual mutation

subcategories. This may lead to overly large apparent variations between background rates of mutation subtypes in different samples. Mutations are shown in the context of UniProt regions and domains (www.uniprot.org). *Post-hoc* analyses for significant non-overlap of *NF2*, *SMO*, and *AKT1* mutations were determined by Fisher's exact test, as were associations between these mutations and chr22 loss or specific categorical demographic characteristics. The Mann-Whitney test was used for comparisons of mutations and continuous demographic variables.

Germline variants were called using UnifiedGenotyper^{45,46}, filtered against the 1000genomes dataset⁵⁰, and annotated to genes as above. Genes with known syndromic associations to meningiomas (*NF1*, *NF2*, *SMARCB1* and *PTCH1*) were manually reviewed for germline non-synonymous mutations. These were visualized in Integrative Genomics Viewer (www.broadinstitute.org/igv/).

Sequenom Validation

We obtained IRB approval for collection of independent archival paraffin-embedded meningioma samples from the Brigham and Women's Hospital Pathology Department. We identified 95 samples from patients that did not overlap with our cohort of 65 tumors, resected between 2005 and 2012. Forty-nine of these were higher-grade meningiomas. Tissue was de-paraffinized and DNA extracted using standard techniques (QIAGEN, Valencia CA). Variants in *SMO* (W535L and L412F) and *AKT1* (E17K) were assayed using Sequenom's homogeneous Mass-Extend (hME) Genotyping system (Sequenom, Inc. San Diego, CA). Bidirectional probes and primers were designed using Sequenom MassARRAY Typer software (v 4.0), and hME genotyping was performed using 5ng of unamplified genomic DNA template per assay pool (maximum of 4 assays per pool).

Immunohistochemistry

Tissue sections were deparaffinized and rehydrated using Xylene and graded alcohols. Endogenous peroxidase activity was blocked with 3% H₂O₂ in 100% ethanol (1:1; 15 minutes). Antigen retrieval was performed with Dako Target Retrieval Solution, pH 6.0 and pressure cooker treatment (120+/-2°C, 15+/-5 psi) for 45 seconds. Sections were incubated with primary antibodies against GAB1 (Abcam ab27439, 1:100x45min), Ki67 (Vector Lab VP-451, 1:2500x45min), or Stathmin (Cell Signaling Technologies #3352, 1:120, 4°Cx16hr), followed by secondary antibody (Dako Labeled Polymer-HRP anti-rabbit IgG x30min). Visualization was with 3,3'-diaminobenzidine as a chromogen (Envision+System) and Gill hematoxylin counterstaining. Associations between specific mutations and their differences in histopathological subtypes and immunohistochemical staining were determined *post-hoc* with Fisher's exact test.

Supplementary Material

Refer to Web version on PubMed Central for supplementary material.

ACKNOWLEDGEMENTS

The authors would like to thank Mike Lawrence, Nicolas Stransky, Marchin Imielinski, Kristian Cibulskis, Scott Carter, Chip Stewart, Cheng-Zhong Zhang, Yotam Drier, Steven Schumacher and Barbara Tabak for their assistance with genomic analyses; Patrick Wen, Ossama Al-Mefty, Tracy Batchelor, Benjamin Reisler, Mark Johnson, William Richards, and James Kim for assisting with tissue acquisition; and Anna Pisarek-Horowitz, Sophie Adele Horowitz, Guillaume Berghold and Charilaos H. Brastianos for critical review of the manuscript. This work was supported by the Brain Science Foundation (I.F.D., P.K.B., R.B., S.S.), Pediatric Low Grade Astrocytoma Foundation (R.B., W.C.H.), American Brain Tumor Association (P.K.B.), Conquer Cancer Foundation Young Investigator Award (P.K.B.), NIH grants K08 CA122833 (R.B.), K08 NS064168 (S.S.), and K12 CA090354-11 (P.K.B.), and Department of Defense grant #W81XWH-12-1-0136 (P.H.).

REFERENCES

1. Choy W, et al. The molecular genetics and tumor pathogenesis of meningiomas and the future directions of meningioma treatments. *Neurosurg Focus*. 2011; 30:E6. [PubMed: 21529177]
2. van Alkemade H, et al. Impaired survival and long-term neurological problems in benign meningioma. *Neuro Oncol*. 2012; 14:658–666. [PubMed: 22406926]
3. Durand A, et al. WHO grade II and III meningiomas: a study of prognostic factors. *J Neurooncol*. 2009; 95:367–375. [PubMed: 19562258]
4. Perry A, Scheithauer BW, Stafford SL, Lohse CM, Wollan PC. "Malignancy" in meningiomas: a clinicopathologic study of 116 patients, with grading implications. *Cancer*. 1999; 85:2046–2056. [PubMed: 10223247]
5. Goutagny S, et al. Genomic profiling reveals alternative genetic pathways of meningioma malignant progression dependent on the underlying NF2 status. *Clin Cancer Res*. 2010; 16:4155–4164. [PubMed: 20682713]
6. Krayenbuhl N, Pravdenkova S, Al-Mefty O. De novo versus transformed atypical and anaplastic meningiomas: comparisons of clinical course, cytogenetics, cytokinetics, and outcome. *Neurosurgery*. 2007; 61:495–503. discussion 503–4. [PubMed: 17881961]
7. Wen PY, Quant E, Drappatz J, Beroukheim R, Norden AD. Medical therapies for meningiomas. *J Neurooncol*. 2010; 99:365–378. [PubMed: 20820875]
8. Bass AJ, et al. Genomic sequencing of colorectal adenocarcinomas identifies a recurrent VTIIA-TCF7L2 fusion. *Nat Genet*. 2011; 43:964–968. [PubMed: 21892161]
9. Berger MF, et al. Melanoma genome sequencing reveals frequent PREX2 mutations. *Nature*. 2012; 485:502–506. [PubMed: 22622578]
10. Berger MF, et al. The genomic complexity of primary human prostate cancer. *Nature*. 2011; 470:214–220. [PubMed: 21307934]
11. Chapman MA, et al. Initial genome sequencing and analysis of multiple myeloma. *Nature*. 2011; 471:467–472. [PubMed: 21430775]
12. Stransky N, et al. The mutational landscape of head and neck squamous cell carcinoma. *Science*. 2011; 333:1157–1160. [PubMed: 21798893]
13. Lohr JG, et al. Discovery and prioritization of somatic mutations in diffuse large B-cell lymphoma (DLBCL) by whole-exome sequencing. *Proc Natl Acad Sci U S A*. 2012; 109:3879–3884. [PubMed: 22343534]
14. Beroukheim R, et al. The landscape of somatic copy-number alteration across human cancers. *Nature*. 2010; 463:899–905. [PubMed: 20164920]
15. Greenman C, et al. Patterns of somatic mutation in human cancer genomes. *Nature*. 2007; 446:153–158. [PubMed: 17344846]
16. Mawrin C, Perry A. Pathological classification and molecular genetics of meningiomas. *J Neurooncol*. 2010; 99:379–391. [PubMed: 20809251]
17. Ketter R, et al. Hyperdiploidy defines a distinct cytogenetic entity of meningiomas. *J Neurooncol*. 2007; 83:213–221. [PubMed: 17225936]
18. Nunes F, et al. Inactivation patterns of NF2 and DAL-1/4.1B (EPB41L3) in sporadic meningioma. *Cancer Genet Cytogenet*. 2005; 162:135–139. [PubMed: 16213361]

19. Rausch T, et al. Genome sequencing of pediatric medulloblastoma links catastrophic DNA rearrangements with TP53 mutations. *Cell*. 2012; 148:59–71. [PubMed: 22265402]
20. Stephens PJ, et al. Massive genomic rearrangement acquired in a single catastrophic event during cancer development. *Cell*. 2011; 144:27–40. [PubMed: 21215367]
21. Takita J, et al. Aberrations of NEGR1 on 1p31 and MYEOV on 11q13 in neuroblastoma. *Cancer Sci*. 2011; 102:1645–1650. [PubMed: 21624008]
22. Yang HW, et al. Alternative splicing of CHEK2 and codeletion with NF2 promote chromosomal instability in meningioma. *Neoplasia*. 2012; 14:20–28. [PubMed: 22355270]
23. Kooistra SM, Helin K. Molecular mechanisms and potential functions of histone demethylases. *Nature reviews. Molecular cell biology*. 2012; 13:297–311. [PubMed: 22473470]
24. Hadfield KD, et al. Molecular characterisation of SMARCB1 and NF2 in familial and sporadic schwannomatosis. *J Med Genet*. 2008; 45:332–339. [PubMed: 18285426]
25. Schmitz U, et al. INI1 mutations in meningiomas at a potential hotspot in exon 9. *Br J Cancer*. 2001; 84:199–201. [PubMed: 11161377]
26. Tsurusaki Y, et al. Mutations affecting components of the SWI/SNF complex cause Coffin-Siris syndrome. *Nat Genet*. 2012; 44:376–378. [PubMed: 22426308]
27. Reifengerger J, et al. Missense mutations in SMOH in sporadic basal cell carcinomas of the skin and primitive neuroectodermal tumors of the central nervous system. *Cancer Res*. 1998; 58:1798–1803. [PubMed: 9581815]
28. Jones DT, et al. Dissecting the genomic complexity underlying medulloblastoma. *Nature*. 2012; 488:100–105. [PubMed: 22832583]
29. Laurendeau I, et al. Gene expression profiling of the hedgehog signaling pathway in human meningiomas. *Mol Med*. 2010; 16:262–270. [PubMed: 20386868]
30. Aavikko M, et al. Loss of SUFU function in familial multiple meningioma. *Am J Hum Genet*. 2012; 91:520–526. [PubMed: 22958902]
31. Gorlin RJ. Nevoid basal-cell carcinoma syndrome. *Medicine (Baltimore)*. 1987; 66:98–113. [PubMed: 3547011]
32. Santos DC, et al. PTCH1 gene mutations in exon 17 and loss of heterozygosity on D9S180 microsatellite in sporadic and inherited human basal cell carcinomas. *Int J Dermatol*. 2011; 50:838–843. [PubMed: 21699520]
33. Bleeker FE, et al. AKT1(E17K) in human solid tumours. *Oncogene*. 2008; 27:5648–5650. [PubMed: 18504432]
34. Wellenreuther R, et al. Analysis of the neurofibromatosis 2 gene reveals molecular variants of meningioma. *Am J Pathol*. 1995; 146:827–832. [PubMed: 7717450]
35. Mathiesen T, Lindquist C, Kihlstrom L, Karlsson B. Recurrence of cranial base meningiomas. *Neurosurgery*. 1996; 39:2–7. discussion 8–9. [PubMed: 8805134]
36. Ellison DW, et al. Medulloblastoma: clinicopathological correlates of SHH, WNT, and non-SHH/WNT molecular subgroups. *Acta Neuropathol*. 2011; 121:381–396. [PubMed: 21267586]
37. Karst AM, et al. Stathmin 1, a marker of PI3K pathway activation and regulator of microtubule dynamics, is expressed in early pelvic serous carcinomas. *Gynecol Oncol*. 2011; 123:5–12. [PubMed: 21683992]
38. Riobo NA, Lu K, Ai X, Haines GM, Emerson CP Jr. Phosphoinositide 3-kinase and Akt are essential for Sonic Hedgehog signaling. *Proc Natl Acad Sci U S A*. 2006; 103:4505–4510. [PubMed: 16537363]
39. Von Hoff DD, et al. Inhibition of the hedgehog pathway in advanced basal-cell carcinoma. *N Engl J Med*. 2009; 361:1164–1172. [PubMed: 19726763]
40. Janku F, et al. PI3K/AKT/mTOR inhibitors in patients with breast and gynecologic malignancies harboring PIK3CA mutations. *J Clin Oncol*. 2012; 30:777–782. [PubMed: 22271473]
41. Parsons DW, et al. An integrated genomic analysis of human glioblastoma multiforme. *Science*. 2008; 321:1807–1812. [PubMed: 18772396]
42. Samuels Y, et al. High frequency of mutations of the PIK3CA gene in human cancers. *Science*. 2004; 304:554. [PubMed: 15016963]

43. Demichelis F, et al. SNP panel identification assay (SPIA): a genetic-based assay for the identification of cell lines. *Nucleic Acids Res.* 2008; 36:2446–2456. [PubMed: 18304946]
44. Li H, Durbin R. Fast and accurate short read alignment with Burrows-Wheeler transform. *Bioinformatics.* 2009; 25:1754–1760. [PubMed: 19451168]
45. DePristo MA, et al. A framework for variation discovery and genotyping using next-generation DNA sequencing data. *Nat Genet.* 2011; 43:491–498. [PubMed: 21478889]
46. McKenna A, et al. The Genome Analysis Toolkit: a MapReduce framework for analyzing next-generation DNA sequencing data. *Genome Res.* 2010; 20:1297–1303. [PubMed: 20644199]
47. Reich M, et al. GenePattern 2.0. *Nat Genet.* 2006; 38:500–501. [PubMed: 16642009]
48. Chiang DY, et al. High-resolution mapping of copy-number alterations with massively parallel sequencing. *Nat Methods.* 2009; 6:99–103. [PubMed: 19043412]
49. Krzywinski M, et al. Circos: an information aesthetic for comparative genomics. *Genome Res.* 2009; 19:1639–1645. [PubMed: 19541911]
50. A map of human genome variation from population-scale sequencing. *Nature.* 2010; 467:1061–1073. [PubMed: 20981092]

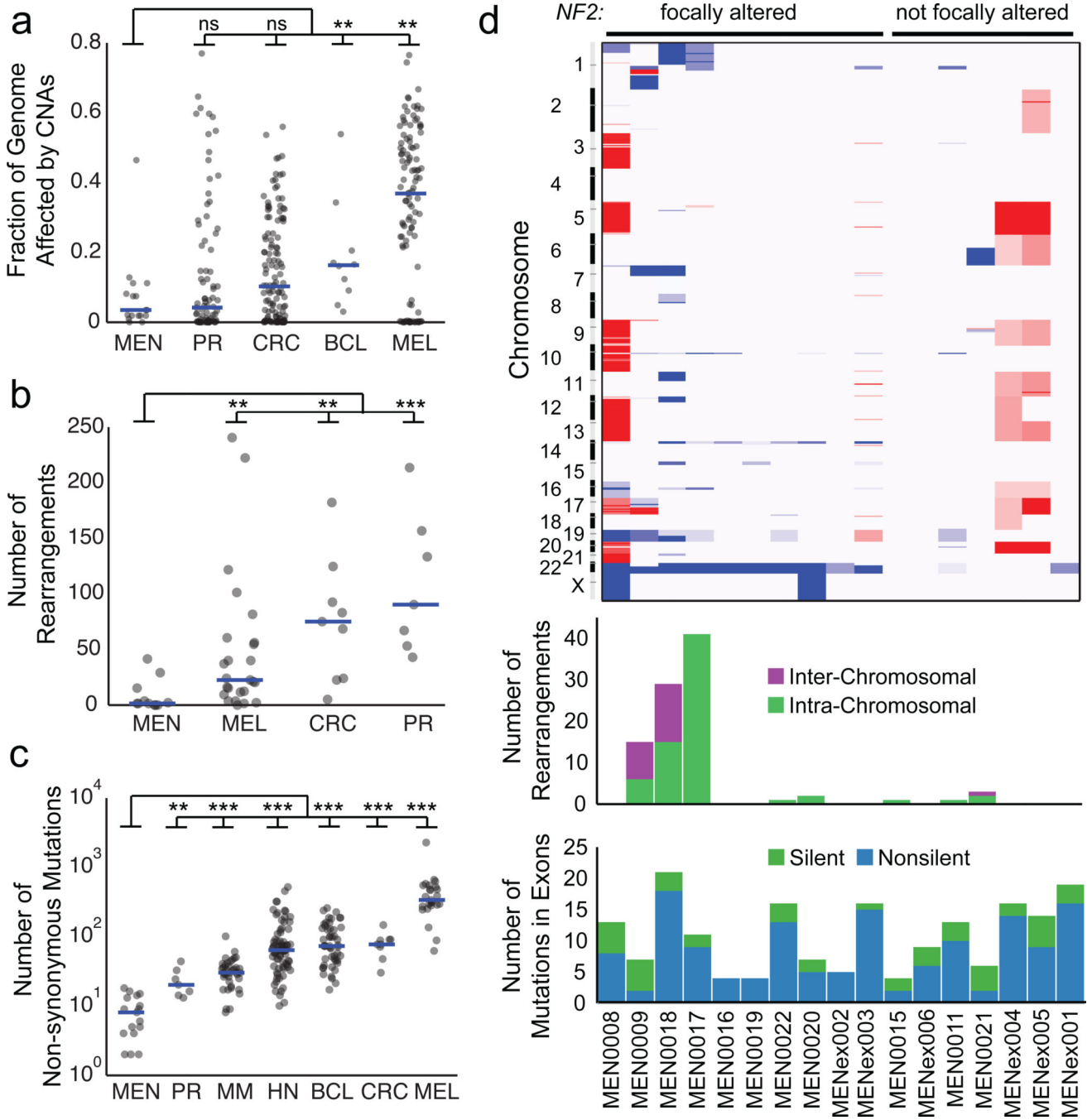


Figure 1.

The landscape of somatic alterations in the grade I meningioma genome. (a) Fraction of the genome altered by somatic copy-number alterations (SCNAs), (b) number of somatic intra- and inter-chromosomal rearrangements, and (c) number of non-synonymous mutations in meningiomas and other tumor types. MEN: meningioma; PR: prostate; CRC: colorectal carcinoma; BCL: diffuse large B-cell lymphoma; MEL: melanoma; MM: multiple myeloma; HN: head and neck cancers. (d) Somatic genetic alterations in individual grade I meningiomas of the discovery cohort. *Top*: Copy-number profiles (red = gain, blue = loss).

Middle: Number of somatic rearrangements per tumor. Samples labeled as MENex are exome-sequenced, in which no rearrangements were detected. *Bottom:* Total non-synonymous and synonymous mutations in exons. ** $p < 0.01$, *** $p < 0.0001$.

Author Manuscript

Author Manuscript

Author Manuscript

Author Manuscript

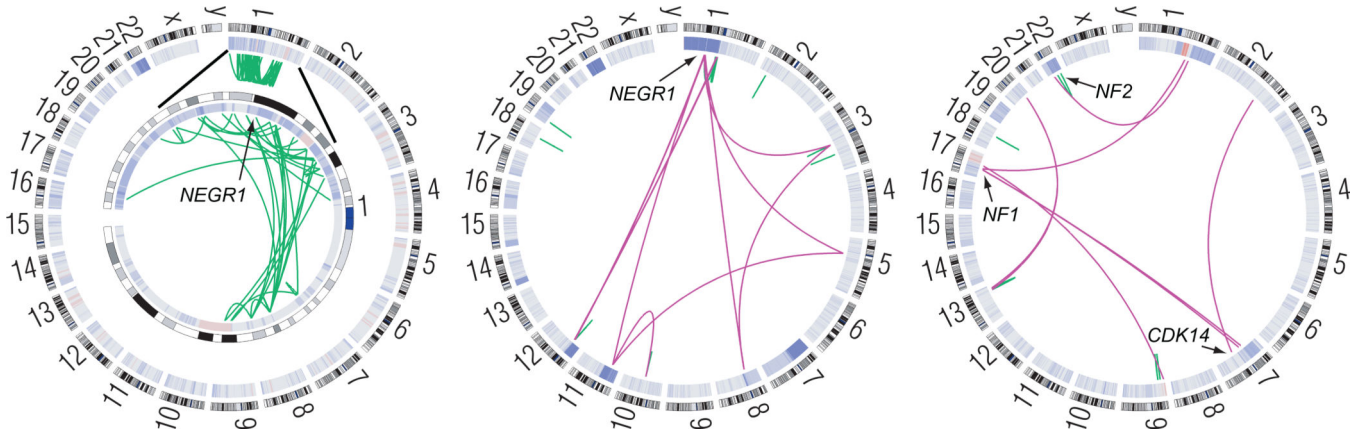


Figure 2. Somatic rearrangements disrupt tumor suppressors in several meningiomas. Circos plots show the SCNAs (inner ring heat map) and intra- and inter-chromosomal rearrangements (green and purple arcs, respectively) in three whole-genome sequenced meningiomas. *Left:* Chromothripsis of chromosome 1 (enlarged in inset) in an *NF2*-mutated sample (MEN0017) disrupts the putative tumor suppressor *NEGR1*. *Middle:* A second *NF2*-mutated sample (MEN0018) harbors 29 rearrangements including disruption of *NEGR1*. *Right:* An inversion on chromosome 22 disrupts *NF2*, and other rearrangements affect *NF1* and *CDK14* (MEN0009). Data from the remaining tumors are shown in Supplementary Figure 4.

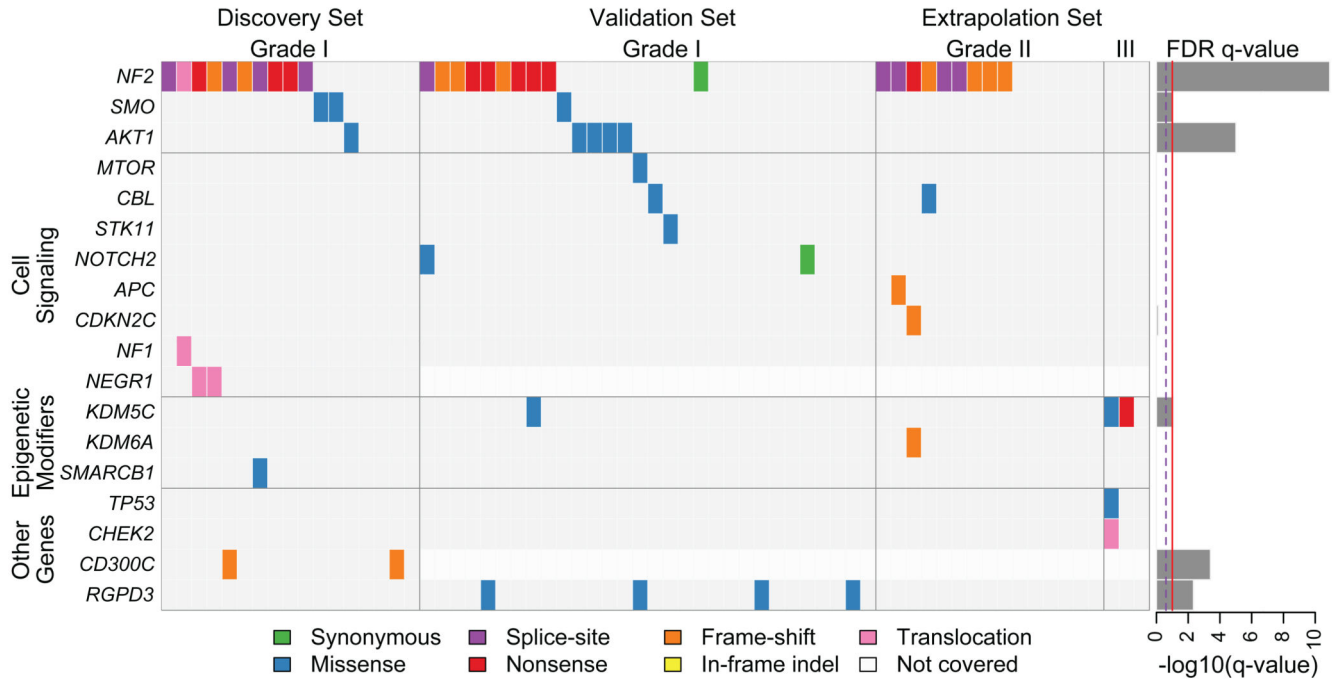


Figure 3. Significant and selected cancer-related somatic mutations, insertion-deletions, and translocations in meningiomas. Mutation subtypes are denoted by the indicated colors. If multiple mutations were found in a gene in a single sample, only one is shown. Discovery set tumors are in the same order as in Figure 1d. *Right:* Significance of mutations in each gene, as false discovery rate q-values. The full list of mutated genes is shown in Supplementary Table 4.

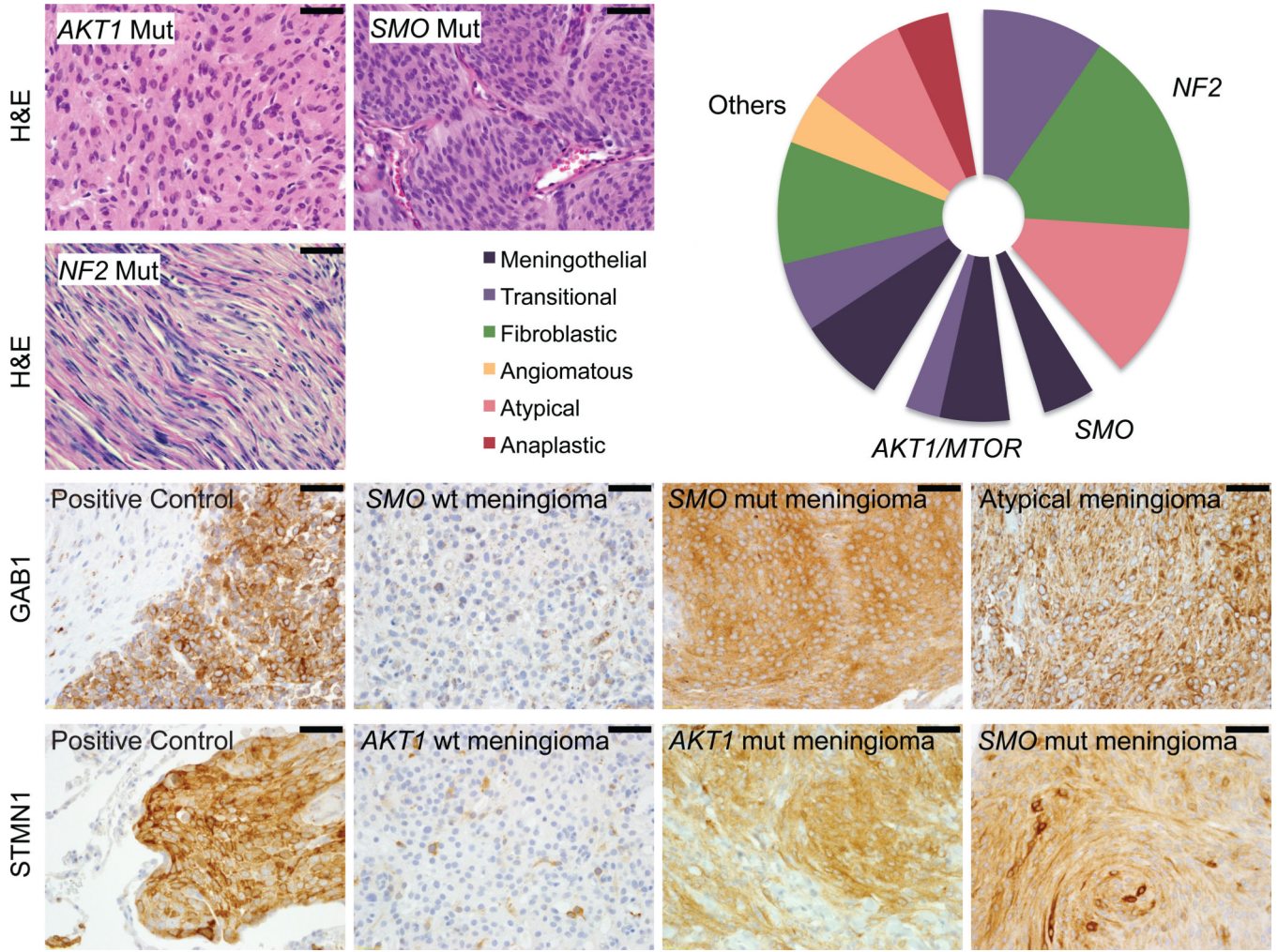


Figure 4. Associations between mutations in Hh and Akt/mTOR pathways and histologic findings. (a) *AKT1/MTOR* and *SMO*-mutated samples are predominantly of the meningeothelial subtype ($p=0.009$, $p=0.005$). *NF2*-mutated samples are predominantly fibroblastic and transitional ($p=0.013$). (b) Immunohistochemistry indicates activation of Hh and Akt/mTOR pathways in tumors harboring *SMO* and *AKT1* mutations, respectively ($p=0.0008$, $p=3 \times 10^{-6}$). GAB1 staining was used as a marker of Hh pathway activation, and STMN1 staining was used as a marker of PI3K/Akt/mTOR pathway activation. Scale bars denote 50 micrometers.